

# VLT/ISAAC and HST/WFPC2 Observations of NGC 3603

B. BRANDL<sup>1</sup>, W. BRANDNER<sup>2</sup>, E.K. GREBEL<sup>3</sup> AND H. ZINNECKER<sup>4\*</sup>

<sup>1</sup>Cornell University, Ithaca; <sup>2</sup>University of Hawaii, Honolulu;

<sup>3</sup>University of Washington at Seattle; <sup>4</sup>Astrophysikalisches Institut Potsdam

## 1. Abstract

We have studied NGC 3603, the most massive visible HII region in the Galaxy, with VLT/ISAAC in the near-infrared (NIR)  $J_s$ , H, and  $K_s$ -bands and HST/WFPC2 at  $H\alpha$  and [NII] wavelengths. In this *Messenger* article we describe the data analysis and some first results from both our complementary observations.

Our HST/WFPC2 gave us an unprecedented high-resolution view of the interstellar medium in the giant HII region and its ionisation structure. Among the findings are two gigantic gas columns (similar to the famous "elephant trunks" in M16) and three proplyd-like structures. The emission nebulae are clearly resolved; all three nebulae are tadpole shaped, with the bright ionisation front at the head facing the central cluster and a fainter ionisation front around the tail pointing away from the cluster. Typical sizes are 6000 A.U.  $\times$  20,000 A.U. The nebulae share the overall morphology of the proplyds ("PROto PLANetarY DiskS") in Orion, but are 20 to 30 times larger in size.

The VLT observations are the most sensitive near-infrared observations made to date of a dense starburst region, allowing us to investigate with unprecedented quality its low-mass stellar population. Our sensitivity limit to stars detected in all three bands corresponds to 0.1  $M_\odot$  for a pre-main sequence star of age 0.7 Myr. Our observations clearly show that sub-solar-mass stars down to at least 0.1  $M_\odot$  do form in massive starbursts.

## 2. Introduction

NGC 3603 is located in the Carina spiral arm (RA = 11h, DEC = -61°) at a distance of 6–7 kpc. It is the only massive, Galactic HII region whose ionising central cluster can be studied at optical wavelengths, due to only moderate (mainly foreground) extinction of  $A_V = 4\text{--}5$  mag (Moffat 1983; Melnick et al. 1989). The OB stars ( $> 10 M_\odot$ ) and stars with the

spectral signatures of Wolf-Rayet (W-R) stars contribute more than 2000  $M_\odot$  to the cluster mass. Normally, W-R stars are evolved supergiants that have long left the main sequence and have ages of 3–5 Myr. In NGC 3603, however, the W-R stars also show hydrogen absorption lines in addition to the typical W-R features. It is believed that these stars are still main-sequence, core hydrogen-burning stars that are so massive and so close to the Eddington limit that they are losing their outer envelopes through fast winds, and thus resemble evolved W-R stars. In comparison to the Orion Trapezium system, NGC 3603 with its more than 50 O and W-R stars producing a Lyman continuum flux of  $10^{51} \text{ s}^{-1}$  (Kennicutt 1984; Drissen et al. 1995) has about 100 times the ionising power of the Trapezium cluster.

With a bolometric luminosity  $L_{\text{bol}} > 10^7 L_\odot$ , NGC 3603 has about 10% of the luminosity of 30 Doradus and looks in many respects very similar to its stellar core R136 (Brandl et al. 1996). In fact, it has been called a Galactic clone of R 136 but without the massive surrounding cluster halo (Moffat, Drissen & Shara 1994). In many ways NGC 3603 and R136 can be regarded as representative building blocks of more distant and luminous starburst galaxies (Brandl, Brandner & Zinnecker 1999, and references therein). So the best way to study collective star formation in a violent environment is by examining these regions on a star-by-star basis. Until recently, observations of the entire stellar populations were limited to the massive stars by sensitivity or wavelength restrictions. The formation of low-mass stars in starburst regions is of particular interest. Fundamental questions that arise in this context are: Does the slope of the IMF vary on small scales? Do low-mass stars in a starburst event form together with the most massive stars or do they form at different times or on different timescales? And finally, one might even ask if low-mass stars form at all in such environments?

In addition, NGC 3603 is an ideal laboratory to study individual (!) star formation. Some young stars in the vicinity of massive stars are surrounded by partially ionised circumstellar clouds with cometary shape, so-called protoplanetary disks ("Proplyds"), ionised from the out-

side (Churchwell et al. 1987; O'Dell et al. 1993). FUV photons (13.6 eV  $> h\nu > 6$  eV) heat up the inside of the proplyd envelope and lead to the dissociation of molecules in the outer layers of the circumstellar disk (Johnstone et al. 1998). The resulting evaporation flow provides a steady supply of neutral atoms to the ionisation front and leads to the development of a cometary tail (McCullough et al. 1995; Störzer & Hollenbach 1999). Until recently, only one other proplyd had been found outside the Orion nebula. It is located in the vicinity of the O7V star Herschel 36 in the Lagoon Nebula (M8, Stecklum et al. 1998).

## 3. VLT/ISAAC Observations

We observed NGC 3603 through the  $J_s = 1.16\text{--}1.32 \mu\text{m}$ , H =  $1.50\text{--}1.80 \mu\text{m}$ , and  $K_s = 2.03\text{--}2.30 \mu\text{m}$  broadband filters using the NIR camera ISAAC on ANTU, the first VLT unit telescope. The observations were made during the 4 nights of April 4–6 and 9, 1999, in service mode when the optical seeing was equal to, or better than, 0.4" in 1-minute exposures. Such seeing was essential for accurate photometry in the crowded cluster and increased our sensitivity to the faintest stars. The majority of our data were taken under photometric conditions.

Our observing strategy was to use the shortest possible frame times of 1.77 seconds to keep the number of saturated stars to a minimum. However, due to the system's excellent sensitivity, about two dozen of the brightest stars ended up being saturated. Nevertheless, this does not impose a problem to our study of the low-mass stars. Thirty-four short exposures were co-added to an effective one-minute exposure, the minimum time per pointing required to stabilise the telescope's active optics control system. Between the 1-minute pointings we moved the telescope by up to 20" offsets in a random pattern. This approach has several advantages:

- Enlargement of the observed field of view (FOV) with maximum signal-to-noise (S/N) in the cluster centre.
- Reduction of residual images and other array artefacts, using the median filtering technique.

\*Our collaborators on the project described in this article are Y.-H. Chu, H. Dottori, F. Eisenhauer, A.F.J. Moffat, F. Palla, S. Richling, H.W. Yorke and S. D. Points.

- Derivation of the “sky” from the target exposures using the median filtering technique. No additional time for “blank” sky frames outside the cluster was required.

The sky frames have been computed using between 15 and 37 subsequent exposures per waveband and night, and careful eye-inspection showed that all sources have been efficiently removed using our modified median filtering technique which returns the lower 1/3 instead of the mean (1/2) value.

We subtracted the sky background and flat-fielded each exposure using the twilight flat-fields provided by ESO. The relative position offsets were derived from cross-correlating the images; the exposures were co-aligned on a  $0.5 \times 0.5$ -pixel sub-grid for better spatial resolution, and then added together using the median filtering technique. The resulting images are  $3.4 \times 3.4$  in

size with pixels of  $0''.074$ . The effective exposure times of the final broadband images in the central  $2.5 \times 2.5$  are 37, 45, and 48 minutes in  $J_s$ , H, and  $K_s$ , respectively.

Figure 1 shows the impressive 3-colour composite image that has recently been the subject of an ESO press release. (<http://www.eso.org/outreach/press-rel/pr-1999/pr-16-99.html>). The brightest star in the FOV ( $80''$  northeast of the core) is the red supergiant IRS 4 (Frogel, Persson, & Aaronson 1977). To the south of the cluster is a giant molecular cloud (GMC). Ionising radiation and fast stellar winds from the starburst cluster are excavating large gaseous pillars. Located about  $20''$  to the north of the cluster centre is the blue supergiant Sher 25. This supergiant is unique because its circumstellar ring and bipolar outflows form an hourglass structure similar to that of SN 1987A (Brandner et al. 1997a, 1997b). The image also shows the three proplyd-like objects that have recently been discovered by Brandner et al. (2000) (see Fig. 2 for



Figure 1: Three-colour image of NGC 3603 composed from  $J_s$  (blue), H (green), and  $K_s$ -band (red) images. Intensities are scaled in logarithmic units. The field of view is  $3.4 \times 3.4$ . North is up, East to the left. The insert to the lower right is a blow-up of the central parsec<sup>2</sup>.

details). About  $1'$  south of the central cluster, we detect the brightest members of the deeply embedded protocluster IRS 9.

In order to derive the photometric fluxes of the stars we used the IRAF implementation of DAOPHOT (Stetson 1987). We first ran DAOFIND to detect the individual sources, leading to  $\approx 20,000$  peaks in each waveband. Many of these may be noise or peaks in the nebular background and appear only in one waveband. In order to reject spurious sources, we required that sources be detected independently in all three wavebands, and that the maximal deviation of the source position centroid between different wavebands be less than  $0.075''$ . The resulting source list contains 6967 objects in the entire FOV. We then flux-calibrated the images using the faint NIR standard stars from the lists by Hunt et al. (1998) and Persson et al. (1998). Because of the stringent requirements on the seeing, the PSF did not noticeably change during our

observations and the systematic photometric errors are dominated by uncertainties in the aperture offsets. (A detailed error analysis will be part of a subsequent paper). Comparing our photometric fluxes of numerous sources with the fluxes derived by Eisenhauer et al. (1998) yields a systematic offset of  $0.1^m$  in  $J_s$  and  $0.05^m$  in  $K_s$ .

#### 4. HST/WFPC2 Observations

On March 5, 1999 we obtained deep narrow-band  $H\alpha$  (F656N,  $2 \times 500s$ ) and [NII] (F658N,  $2 \times 600s$ ) observations. The Planetary Camera (PC2) chip was centred on the bipolar outflow structure around the blue supergiant Sher 25. The three Wide Field Camera (WF) chips covered the central cluster and the HII region to the South of Sher 25. In addition, we retrieved and analysed archival HST data, which had originally been obtained in July 1997 (PI Drissen). The

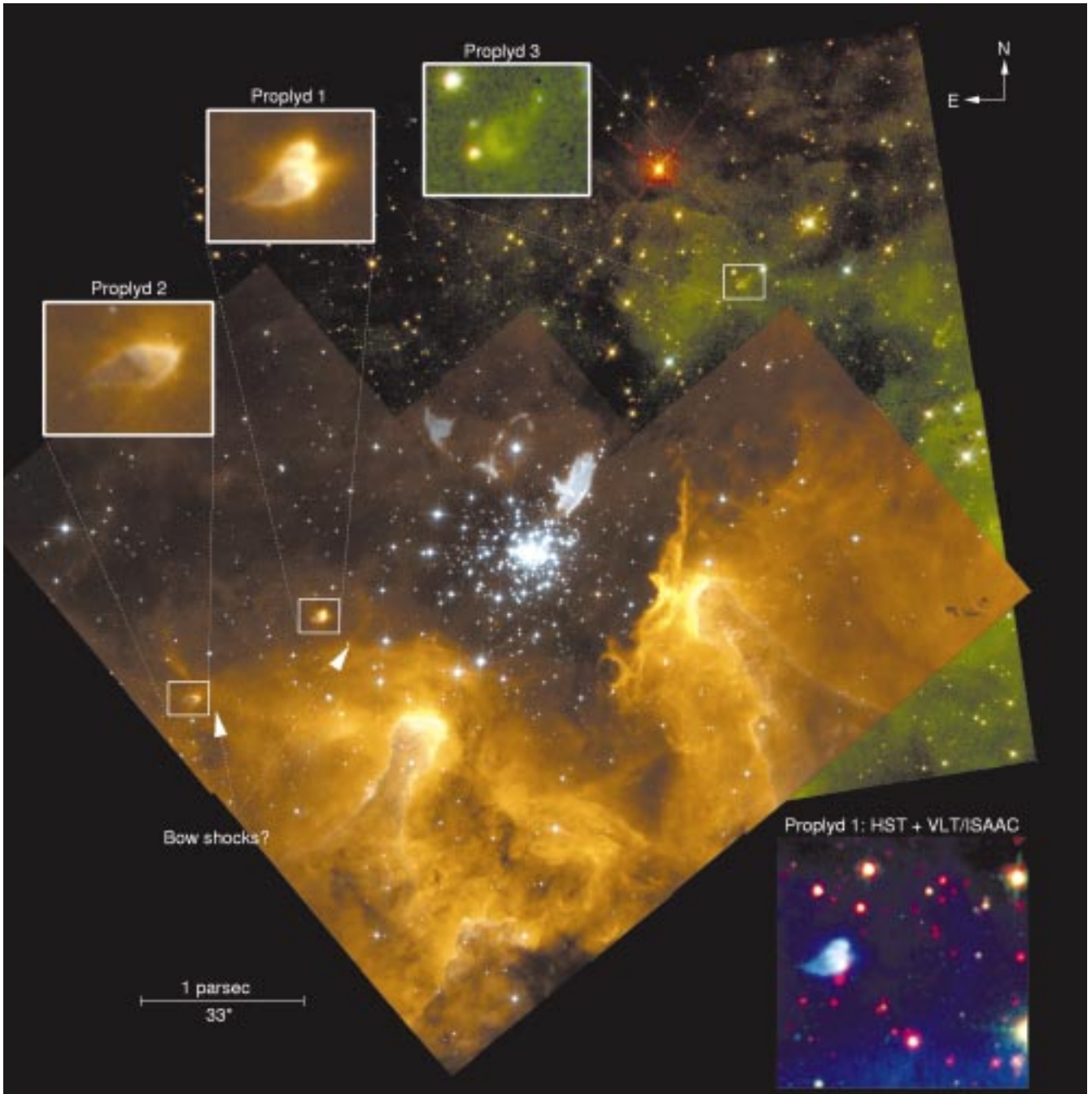


Figure 2: WFC2 observations of NGC 3603. North is up and East is to the left. The upper part of the image consists of the archive data with the following colour coding: F547M (blue), F675W (green), F814W (red). Overlaid are our new WFC2 data with the F656N data in the red channel, the average of F656N and F658N in the green channel, and F658N in the blue channel. The location of the three proplyd-like emission nebulae is indicated. The insert at the lower right is a combination of WFC2 F656N (blue) and F658N (green) and VLT/ISAAC Ks (red) observations.

PC2 was centred on the cluster, and the three WF chips covered the area north-west of the cluster. We combined individual short exposures in F547M ( $8 \times 30$ s), F675W ( $8 \times 20$ s), and F814W ( $8 \times 20$ s) to produce images with effective exposure times of 240s, 160s, and 160s, respectively.

The HST/WFC2 observations are presented in Figure 2. The figure shows an overlay of two composite colour images. The upper part of the image consists of the archive data with the following colour coding: F547M (blue), F675W (green), F814W (red). Overlaid are our new WFC2 data with

the F656N data in the red channel, the average of F656N and F658N in the green channel, and F658N in the blue channel. The locations of the proplyds are marked by small boxes, and enlargements of the boxes are shown in the upper part of Figure 2. Proplyd 3 has only been observed in intermediate and broad-band filters and thus stands out less clearly against the underlying background when compared to Proplyds 1 and 2. The insert at the lower right shows a colour composite of HST/WFC2 F656N (blue) and F658N (green) data and VLT/ISAAC  $K_s$  data (red).

## 5. Results and Interpretation

All three proplyds are tadpole shaped and rim brightened, with the extended tails facing away from the starburst cluster. The portion of the ionised rims pointing towards the cluster are brighter than the rims on the opposite side. The central parts of the proplyds are fainter than the rims, with a noticeable drop in surface brightness between the head and the tail. Proplyds 2 and 3 exhibit a largely axisymmetric morphology, whereas Proplyd 1, which is also the one closest to the cluster, has a more complex structure. Un-

like the convex shape of the heads of the other proplyds, Proplyd 1 has a heart-shaped head with a collimated, outflow-like structure in between. One possible explanation for the more complex morphology of Proplyd 1 might be that it is actually a superposition of two (or maybe even three) individual proplyds or that the photoevaporative flows of several disks in a multiple system interact to produce this complex single structure.

At distances of 7.4" and 2.9" from Proplyd 1 and 2, respectively, faint arc-like H $\alpha$  emission features are seen on the WFPC2 frames. The arcs are located in the direction of the cluster, and may be the signatures of bow shocks created by the interaction of proplyd winds with the winds from the massive stars in the central cluster. Additional faint filaments located between the nebulae and the central ionising cluster can be interpreted as bow shocks resulting from the interaction of the fast winds from the high-mass stars in the cluster with the evaporation flow from the proplyds.

Low-resolution spectra obtained with EFOSC2 at the ESO/MPI 2.2-m telescope of the brightest nebula, which is at a projected separation of 1.3 pc from the cluster, reveal that it has the spectral excitation characteristics of an ultra compact H II region with electron densities well in excess of  $10^4 \text{ cm}^{-3}$ . The near-infrared data reveal a point source superimposed on the ionisation front.

The striking similarity of the tadpole-shaped emission nebulae in NGC 3603 to the proplyds in Orion suggests that the physical structure of both types of objects might be the same. Our hydrodynamical simulations (Brandner et al. 2000) reproduce the overall morphology of the proplyds in NGC 3603 very well, but also indicate that mass-loss rates of up to  $10^{-5} \text{ Mo yr}^{-1}$  are required in order to explain the size of the proplyds. Due to these high mass-loss rates, the proplyds in NGC 3603 should only survive  $10^5$  yrs. Despite this short survival time, we detect three proplyds. This indicates that circumstellar disks must be common around young stars in NGC 3603 and that these particular proplyds have only recently been exposed to their present harsh UV environment.

The point source close to the head of Proplyd 3 is already detected on the broadband HST/WFPC2 observations (see Figure 2). The WFPC2 images show that the point source is actually located in front of Proplyd 3 and thus very likely not physically associated with it. The infrared source in Proplyd 1 is also detected as an underlying, heavily reddened continuum source in the spectrum. A more detailed analysis of ground based optical images and spectra of the proplyds and other compact nebulae in NGC 3603 will be presented in Dottori et al. (2000).

The figure on page 1 of this issue of *The Messenger* shows the resulting colour-magnitude diagrams (CMD) de-

rived from our VLT data. The left plot contains all stars detected in all 3 wavebands within the entire FOV of  $3.4 \times 3.4$  (6 pc  $\times$  6 pc). Since NGC 3603 is located in the Galactic Plane we expect a significant contamination from field stars. To reduce this contribution we followed a statistical approach by subtracting the average number of field stars found in the regions around the cluster at  $r > 75''$  (central plot) per magnitude and per colour bin (0.5 mag each).

The accuracy of our statistical subtraction is mainly limited by three factors: first, we cannot rule out that low-mass pre-main-sequence stars are also present in the outskirts of the cluster. Second, because of crowding on one hand and dithering which leads to shorter effective integration times outside the central  $2.5 \times 2.5$  on the other hand, the completeness limit varies across the FOV. Third, local nebulosities may hide background field stars. However, none of these potential errors affects our conclusions drawn from the CMD. The resulting net CMD for cluster stars within  $r < 33''$  of NGC 3603 is shown at the right in the figure on page 1. We overlaid the theoretical isochrones of pre-main sequence stars from Palla & Stahler (1999) down to  $0.1 M_{\odot}$ . We assumed a distance modulus of  $(m-M)_{\odot} = 13.9$  based on the distance of 6 kpc (De Pree et al. 1999) and an average foreground extinction of  $A_V = 4.5^m$  following the reddening law by Rieke & Lebofski (1985).

Applying the isochrones to measured magnitudes could be misleading since the theoretical calculations include only stellar photospheres while the stars still may be surrounded by dust envelopes and accretion disks. This would lead to excess emission in the NIR and make the stars appear younger than they actually are. Typical excess emission of classical T-Tauri stars in the Taurus-Auriga complex have been determined as  $DH = 0.2^m$ , and  $DK = 0.5^m$  (Meyer, Calvet & Hillenbrand 1997). The upper part of the cluster-minus-field CMD clearly shows a main sequence with a marked knee indicating the transition to pre-main-sequence stars. The turn-on occurs at  $J_s \approx 15.5$  mag ( $m \approx 2.9 M_{\odot}$ ). Below the turn-on the main-sequence basically disappears. We note that the width of the pre-main sequence in the right part of the figure on page 1 does not significantly broaden toward fainter magnitudes, indicating that our photometry is not limited by photometric errors. The scatter may in fact be real and due to varying foreground extinction, infrared excess and evolutionary stage. In that case the left rim of the distribution would be representative of the "true" colour of the most evolved stars. Fitting isochrones to the left rim in the CMD yields an age of only 0.3–1.0 Myr. Our result is in good agreement with the study by Eisenhauer et al. (1998) but extends

the investigated mass range by about one order of magnitude toward smaller masses and covers also a much larger area.

Because of  $\approx 10$  magnitudes range in luminosities in the crowded core region, our sensitivity limits of  $J_s \approx 21^m$ ,  $H \approx 20^m$  and  $K_s \approx 19^m$  don't appear to be exceedingly faint (and are about 3 magnitudes above ISAAC's detection limit for isolated sources). However, only VLT/ISAAC's high angular resolution, PSF stability, and overall sensitivity enabled us to study the sub-solar stellar population in a starburst region on a star-by-star basis.

**Acknowledgements:** We would like to thank the ESO staff, in particular those involved in the service observations, for their excellent work.

## References

- Brandl, B., et al. 1996, *ApJ*, **466**, 254.  
 Brandl, B., Brandner, W. & Zinnecker, H. 1999, *Star Formation 1999*, eds. T. Nakamoto et al., in press.  
 Brandl, B., et al. 1999, *A&A Letters*, **352**, L69.  
 Brandner, W., et al. 1997a, *ApJ*, **475**, L45.  
 Brandner, W., et al. 1997b, *ApJ*, **489**, L153.  
 Brandner, W., et al. 2000, *AJ*, in press (January 2000 issue).  
 Churchwell, E., Felliw, M., Wood, D.O.S. & Massi, M. 1987, *ApJ*, **321**, 516.  
 De Pree, C.G., Nysewander, M.C. & Goss, W.M. 1999, *AJ*, **117**, 2902.  
 Dottori, H., et al. 2000, *subm. to A&A*.  
 Drissen, L., Moffat, A.F.J., Walborn, N. & Shara, M.M. 1995, *AJ*, **110**, 2235.  
 Eisenhauer, F., Quirrenbach, A., Zinnecker, H. & Genzel, R. 1998, *ApJ*, **498**, 278.  
 Frogel, J.A., Persson, S.E., Aaronson, M. 1977, *ApJ*, **213**, 723.  
 Hunt, L.K., et al. 1998, *AJ*, **115**, 2594.  
 Johnstone, D., Hollenbach, D. & Bally, J. 1998, *ApJ*, **499**, 758.  
 Kennicutt, R.C. Jr. 1984, *ApJ*, **287**, 116.  
 McCullough, P.R., Fugate, R.Q., Christou, J.C. et al. 1995, *ApJ*, **438**, 394.  
 Melnick, J., Tapia, M. & Terlevich, . 1989, *A&A*, **213**, 89.  
 Meyer, M.R., Calvet, N., & Hillenbrand, L.A. 1997, *AJ*, **114**, 288.  
 Moffat, A.F.J. 1983, *A&A*, **124**, 273.  
 Moffat, A.F.J., Drissen, L., & Shara, M.M. 1994, *ApJ*, **436**, 183.  
 O'Dell, C.R.O., Wen, Z. & Hu, X. 1993, *ApJ*, **410**, 686.  
 Palla, F. & Stahler, S.W. 1993, *ApJ*, **418**, 414.  
 Palla, F. & Stahler, S.W. 1999, *ApJ*, in press (20 Nov).  
 Persson, S.E. et al. 1998, *AJ*, **116**, 247.  
 Stecklum, B., Henning, T., Feldt, M., et al. 1998, *ApJ*, **115**, 767.  
 Stetson, P.B. 1987, *PASP*, **99**, 191.  
 Störzer, H. & Hollenbach, D. 1999, *ApJ*, **515**, 669.  
 Zinnecker, McCaughrean & Wilking 1993, *Protostars and Planets III*, eds. E.H. Levy & J.I. Lunine (University of Arizona Press), 429.

E-mail: brandl@astrosun.tn.cornell.edu